Immersive Wave Control Experiments Using Non-isotropic Sources: Laboratory Applications

Xun Li, Theodor Becker, Nele Börsing, Dirk-Jan Van Manen, Andrew Curtis Curtis, Johan Robertsson

IMMERSIVE WAVE CONTROL EXPERIMENTS USING NON-ISOTROPIC SOURCES: LABORATORY APPLICATIONS

Xun Li[1] **Theodor Becker**[1] **Nele Börsing**[1]
Dirk-Jan van Manen[1] **Andrew Curtis**[2] **Johan Robertsson**[1]
[1] ETH Zurich, Sonneggstrasse 5, 8092 Zurich, Switzerland
[2] University of Edinburgh, The King's Building, James Hutton Road, EH9 3FE Edinburgh, UK
xun.li@erdw.ethz.ch

ABSTRACT

A physical experiment can be fully linked and immersed within a virtual (numerical) domain through the real-time exchange of boundary conditions between the experiment and the numerical simulation. Such immersive wave control experimentation relies on active sources deployed around a physical domain (e.g., a water tank) to change its boundary condition. However, in theory, the control algorithm requires sources with an isotropic radiation pattern, while physical sources typically exhibit angle-dependent radiation characteristics. This discrepancy can be overcome by a processing method carried out in the frequency-wavenumber (f-k) domain if the source radiation pattern is known. Here we show the measured radiation pattern of a custom-built Bender-mode X-spring (BMX) type piezoelectric source that will be used in underwater acoustic immersive wave experimentation. We measure the half-space radiation pattern of the BMX source that is mounted at the center of a steel plate with a transversely deployed planar receiver surface. The acquired data is redatumed to that corresponding to receivers deployed along a semi-circle and the source at the origin. The BMX source shows a non-negligible radiation pattern with the highest energy at normal and decreasing power gradually to its perpendicular. The measured radiation pattern will be incorporated into the 3-D physical implementation of immersive wave experimentation.

1. INTRODUCTION

For laboratory wave propagation experimentation, the concept of immersive boundary conditions [1] has emerged in recent years, originating from the method of exact boundary conditions used in numerical modeling [2, 3]. Immersive wave experimentation involves deploying active sources around the physical boundary of a closed domain (e.g., water tank), enabling to fully immerse the domain into a surrounding virtual medium. Figure 1 shows a two-dimensional (2-D) setup for immersive experimentation where sources on the active boundary S^{emt} cancel outgoing waves (e.g., ray path 1 or its reflection along ray path 3) and produce in-going waves (e.g., ray path 4) that result from the wavefield interactions with the surrounding virtual medium. The produced in-going waves are also canceled when arriving at S^{emt}. Wave cancellation and production apply to first and higher-order scattered waves between the physical and virtual domains, producing an illusion within the physical domain that waves propagate seamlessly in the combined two domains.

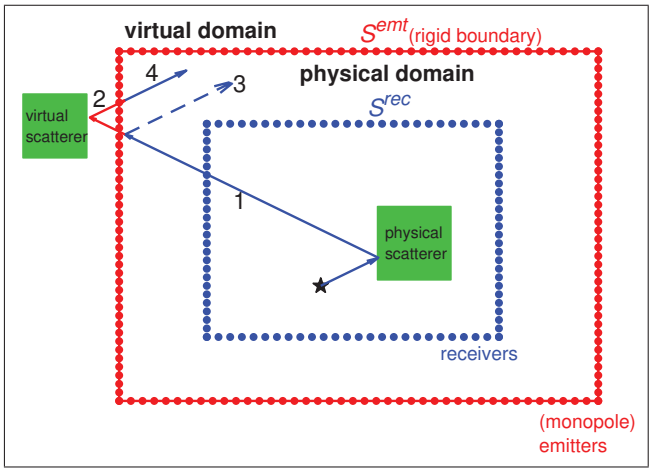

Figure 1. Schematic of immersive wave experimentation. The setup includes (1) a recording surface S^{rec} consisting of closely spaced receivers (blue dots), (2) a rigid boundary (red rectangle) surrounding the physical domain, (3) emitters (red dots) mounted on the rigid boundary (i.e., emitting surface S^{emt}). The black star denotes an internal source generating wavefields for acoustic experiments.

Such a physical laboratory for immersive wave control experimentation is currently constructed in the Exploration and Environmental Geophysics Group at the Swiss Federal Institute of Technology (ETH), Zurich. Immersive boundary conditions have been physically implemented in an air-filled 1-D waveguide as a proof-of-concept [4] and also in a 2-D acoustic waveguide between two closely-spaced plates [5, 6] while for a 3-D domain such as a water tank, the implementation is on-going work. For that purpose, custom-built acoustic piezoelectric sources, pressure hydrophones, amplifiers, and a high-performance computing and control unit based on field-programmable gate array (FPGA) have been manufactured and undergone extensive testing [7].

Immersive wave experimentation requires monopolar sources deployed on the emitting surface S^{emt} in

Fig. 1. However, a physical source (e.g., a piezoelectric transducer) projects waves that do not conform to the theoretically-required monopolar radiation pattern, which causes controlled wavefields to deviate from those desired, especially at high emitting frequencies for which source directivity is typically more pronounced than at low frequencies ($<$ 1 kHz). Ref. [8] proposed a frequency-wavenumber (f-k) processing method that can compensate for the source radiation pattern in immersive wave experimentation. The method involves incorporating the measured source radiation pattern into the pre-computed Green's functions used for wavefield extrapolation, which has been validated in a 2-D synthetic experiment with control sources on S^{emt} that exhibit non-monopolar radiation patterns [8].

In this paper, we show the radiation pattern of a BMX source and discuss the practical application of the source directivity compensation method. In Section 2, we review the theory of immersive boundary conditions that can account for source radiation pattern. We then show the acquisition geometry for measuring the radiation pattern of a BMX source in the laboratory and introduce the necessary processing methods for obtaining the radiation pattern from the measurement. In Section 3, we show the measured radiation pattern, and in Section 4, we discuss the practical usage of these directive sources in immersive wave experimentation. We conclude the paper with an outlook for building a 3-D laboratory for immersive wave experimentation in Section 5.

2. METHOD

2.1 Immersive wave experimentation

Active sources surrounding a closed rigid boundary can fully control the acoustic wavefield inside based on the following IBC term [9]:

$$P^{IBC}(\mathbf{x}',t) = -\int_{S^{emt}} G^p(\mathbf{x}',t,\mathbf{x}_{emt},0) * v_{\mathbf{n}}(\mathbf{x}_{emt},t)\,\mathrm{d}S \tag{1}$$

where the Green's function $G^p(\mathbf{x}',t,\mathbf{x}_{emt},0)$ denotes a pressure source at $\mathbf{x}_{emt}$ (at time 0) and a pressure receiver at an arbitrary point $\mathbf{x}'$ inside the experimental domain. The normal to the emitting surface S^{emt} is denoted by $\mathbf{n}$, and the symbol $*$ refers to convolution in time t. Eqn. (1) implies that the time signatures for these boundary sources at $\mathbf{x}_{emt}$ are the normal particle velocities $v_{\mathbf{n}}(\mathbf{x}_{emt},t)$ of the waves that *have* traveled seamlessly between the physical and virtual domains, without scattering caused by the rigid boundary.

The normal particle velocity $v_{\mathbf{n}}$ [in Eqn. (1)] at S^{emt} is extrapolated from the interior propagating waves (i.e., particle velocities and pressures at the recording surface S^{rec}) using the Kirchhoff-Helmholtz integral [2, 10]:

$$v_{\mathbf{n}}(\mathbf{x}_{emt},t) = \int_{S^{rec}} [G(\mathbf{x}_{emt},t,\mathbf{x}_{rec},0) * v_{\mathbf{m}}(\mathbf{x}_{rec},t) + \Gamma(\mathbf{x}_{emt},t,\mathbf{x}_{rec},0) * p(\mathbf{x}_{rec},t)] \cdot \mathbf{m}\,\mathrm{d}S. \tag{2}$$

Here, G and Γ are the monopolar and dipolar Green's functions, respectively, with direction $\mathbf{m}$ normal to S^{rec}. In a physical experiment, Eqn. (2) is computed in real time such that the wavefield extrapolation is faster than waves traveling between S^{rec} and S^{emt} [4].

As previously noted, physical control sources may exhibit non-isotropic radiation characteristics and hence do not comply with the theory of immersive boundary conditions, which require monopolar sources deployed on the rigid boundary [as denoted by G^p in Eqn. (1)]. To compensate for the source radiation pattern, Ref. [8] apply a f-k processing method to the pre-computed Green's functions in Eqn. (2). Here for simplicity, we only show the processing scheme for the monopolar Green's function G, and the same procedure applies to the dipolar Green's function Γ. We show the f-k processing method in a 2-D geometry which can be extended to a 3-D laboratory application.

We start by (Fourier) transforming the Green's function $G(\mathbf{x}_{emt},t,\mathbf{x}_{rec},0)$ in Eqn. (2) to the frequency-wavenumber (f-k) domain denoted by $\hat{G}(k,f,\mathbf{x}_{rec})$. The spatial axis $\mathbf{x}_{emt}$ corresponds to wavenumber k while t corresponds to frequency f. We then process the transformed $\hat{G}$ in the f-k domain:

$$\hat{\tilde{G}}(k,f,\mathbf{x}_{rec}) = \hat{G}(k,f,\mathbf{x}_{rec})\hat{W}(\pi-\theta,f) \tag{3}$$

where $\hat{W}(\pi-\theta,f)$ are the directive matched filters in the frequency domain (denoted by the symbol $\hat{}$), and the angle $\pi-\theta$ implies that the compensation of the source radiation pattern applies in the direction of wave reflection at the active source boundary S^{emt} for out-going waves (ray path 3 in Fig. 1), and this compensation works also well for in-going waves (see Ref. [8]). Provided that S^{emt} is composed of planer surfaces, the angle θ is given as $\theta = \pi/2 + \arcsin(ck/f)$ where c is the wavespeed of the medium (i.e., water).

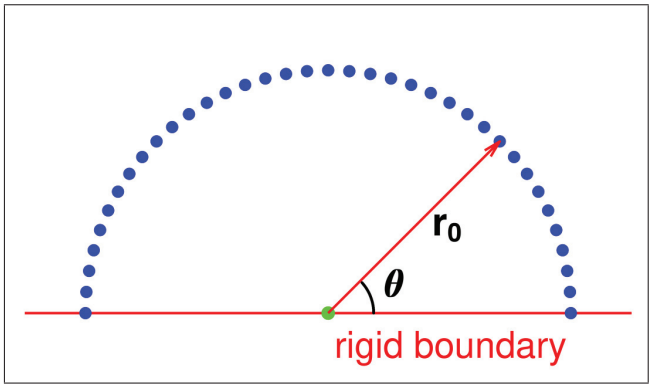

Figure 2. Ideal geometry for the measurement of source radiation patterns (2-D view). The green dot denotes the source mounted on a rigid boundary while the blue dots (hydrophones) are arranged along a semi-circle (or a hemisphere in 3-D) with the same distance r_0 to the source.

Ideally, the radiation pattern can be measured as pressure responses in different directions θ with the geometry shown in Fig. 2. The directive matched filters are calculated from the trace-to-trace deconvolution between the

signals received in different directions θ from a physical directive source in the laboratory $\tilde{M}^p(\theta, f)$ and the counterpart analytical signals from a perfect monopolar source $\tilde{M}^p(\theta, f)$.

$$\hat{W}(\theta, f) = M^p(\theta, f)/\tilde{M}^p(\theta, f). \quad (4)$$

Finally, the processed Green's functions G (and also Γ) in Eqn. (3) are transformed back to the time-space (t-x) domain and further used in wavefield extrapolation [Eqn. (2)] such that source directivity is compensated.

2.2 Acquisition geometry for radiation patterns

Figure 3 shows the piezoelectric sources and pressure-sensitive hydrophones that are used in 3-D immersive wave experimentation [7]. The pressure-sensitive receivers on the recording surface are custom-built piezoelectric hydrophones with negligible directivity [7]. The sources are Bender mode X-spring (BMX) type of piezoelectric transducers, which can generate acoustic waves with high output power across the frequency range 1-20kHz [11–13]. These BMX transducers are mounted flush in a rigid steel plate, which must be included in the measurement of source directivity due to its influence on the radiation pattern [8]. The BMX source is built in close collaboration with the Walker Department of Mechanical Engineering at the University of Texas (UT) at Austin and the Applied Research Laboratories UT Austin [11].

Instead of using the ideal acquisition geometry in Fig. 2, we use the geometry shown in Fig. 4 where one active BMX source emits waves at the center of the rigid steel plate with the receivers arranged in the X-Y plane that contains the source. This measurement only works for source radiation pattern with transverse isotropy, which can be inferred from the manufacture of the BMX source with round front face, shown in Fig. 3(c). Hence, directivity only exists along the direction towards the normal of the emitting surface (or the front face of the source) [7, 11]. Figure 5 shows the locations of the source and receivers in the X-Y plane, and this geometry covers a large (angular) aperture to characterize the source radiation pattern.

2.3 Redatuming of recorded data

The Cartesian coordinate for the locations of the source and receivers in Fig. 5 can be transformed into the radiation angle θ against the source-receiver distance as shown in Fig. 6. Here, we follow a spherical wave spreading model [14]:

$$p(\omega, r) = \frac{S(\omega)e^{-ikr}}{r} \quad (5)$$

where $p(\omega, r)$ is the pressure recorded at distance r from a point source, i is the imaginary unit, and $S(\omega)$ is the frequency spectrum of the source signature. We redatum the recorded data to the semi-circle (as shown in Fig. 2) with radius $r_0 = 0.45$ m:

$$p_c(\omega, r_0) = p(\omega, r)\frac{r_0}{r}e^{ik(r_0 - r)} \quad (6)$$

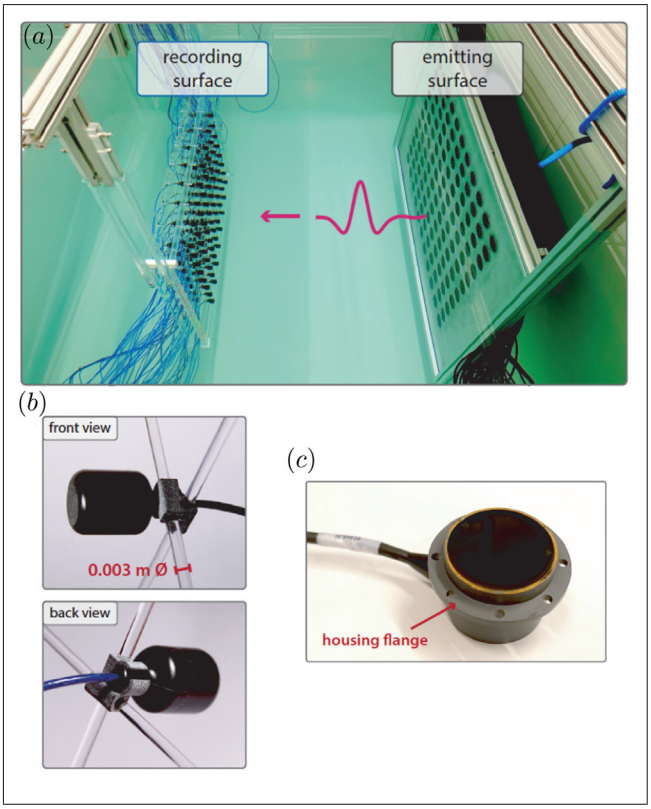

Figure 3. (a) Photo of one-sided immersive wave experimentation containing planar source and receiver arrays in a 3-D water tank. (b) Pressure-sensitive hydrophones (receivers) with front and back views. These receivers are held by a lattice of 3 mm-thick rods. (c) Bender-mode X-spring piezoelectric source with the housing flange (5 cm diameter).

where $p_c(\omega, r_0)$ is the pressure after redatuming. Finally, the results are transformed back to the time domain to yield $p_c(t, r_0)$. The amplitude and phase variation of $p_c(t, r_0)$ in different directions θ represent the source radiation pattern.

3. RESULTS

Figures 7(a) and (b) show the data measured in underwater experiments using the geometry given in Fig. 4 and the data redatumed using Eqn. (6), respectively. The source signature of the BMX source is a Ricker wavelet with peak frequency 6 kHz, and the wavespeed of water is $c = 1488$ m/s. The first events in the redatumed time series [Fig. 7(b)] have almost identical arrival times, indicating that the propagation of direct waves in the water tank is well described by the spherical spreading model.

A strong ringing effect does exist after the expected first arrival in the recorded data. This ringing is undesired and pollutes the measurement of the phase variation in different directions, complicating the estimation of the source radiation pattern. Hence, Eqn. (4) can be further simplified, and we only focus on the amplitude variation for the radiation pattern. For the redatumed data shown in Fig. 7(b), we first calculate the envelope using Hilbert transform [15], which eliminates the phase variation in different directions. The

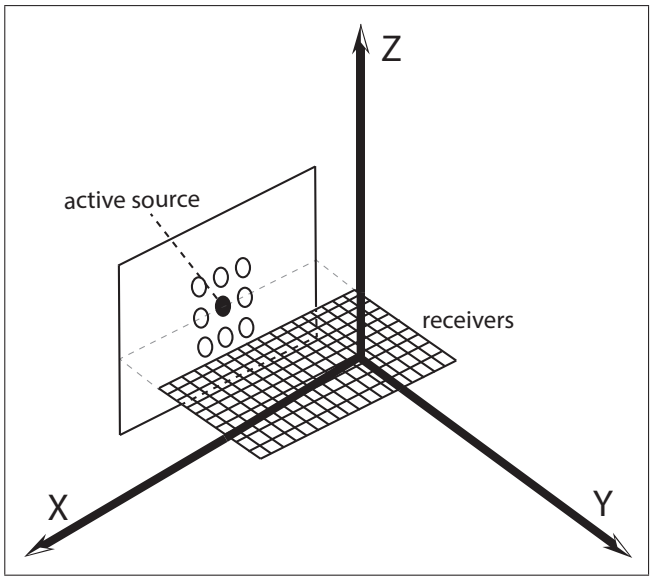

Figure 4. Actual geometry used to measure the radiation pattern of a BMX source in the underwater acoustic laboratory. The planar receiver array is on the same X-Y plane (or same Z-level) with the active source.

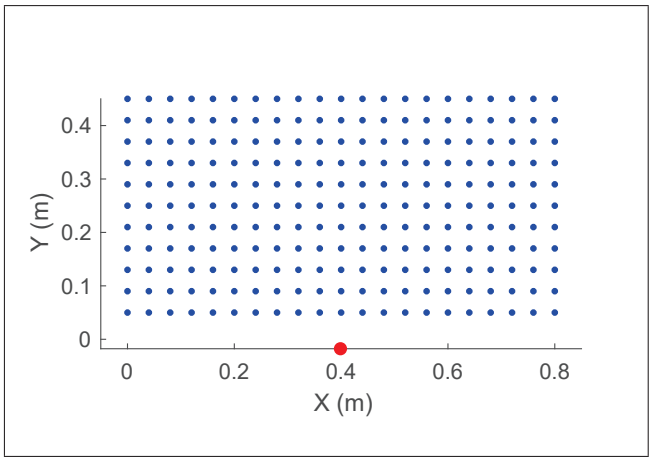

Figure 5. Geometry used to measure the radiation pattern of a BMX source, with view on X-Y plane. The red dot denotes the active BMX source and blue dots denote the receivers.

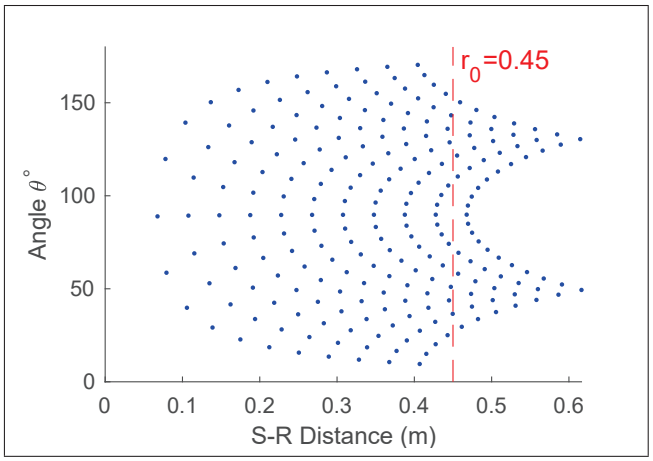

Figure 6. The radiation angles θ against source-receiver (S-R). The red dashed line denotes the reference radius (or source-receiver distance) to which the received signals are redatumed.

maximum amplitude values of these envelopes are plotted against the directions θ, as shown in Fig. 8. This radiation pattern is symmetric with maximum energy in the normal direction ($\theta = 90°$) and decreasing emitted energy to its perpendicular, which is expected in a BMX type source [11]. We also verify that the change of the redatuming radius r_0 does not change the shape of the amplitude variation trend in Fig. 8 (not shown here).

The obtained radiation pattern in Fig. 8 is not evenly sampled in the radiation angle θ. To overcome this fact, we interpolate the acquired pressure data for equally spaced radiation angles using Modified Akima Cubic Hermite interpolation [16, 17], and repeat the estimation of the source radiation pattern, as shown in Fig. 9. The radiation angles θ are resampled with $1°$ interval from $\theta = 10°$ to $170°$.

4. DISCUSSION

The radiation pattern of transducers typically depends on the signal frequency or wavelength. As for wavelengths on the order of the transducer dimensions, the geometry of the source affects the radiation pattern [8]. Hence, the compensation of the source directivity is frequency-dependent, and the frequency range of the measurement of the radiation pattern must match the operating frequency range of immersive experimentation.

The ringing tails that exist in the recorded data [Fig. 7(b)] may not be suppressed or compensated by the proposed deconvolution in Eqn. (4) and is considered as artefacts, which should be removed from the data. Naive deconvolution between the data with ringing tails and the analytical traces results in the directive matched filters that if convolving with the pre-computed Green's functions, generate undesired source emission at the emitting surface S^{emt}. This ringing effect is probably caused by the (nonlinear) coupling between the rigid steel boundary and the physical source and hence cannot be removed by a linear filter. Considering this source characteristic, we plan to first compensate for the amplitude variation in the measured source radiation pattern. The deconvolution in Eqn. (4) becomes a simple division, and the directive matched filters become scalars/ratios varying for waves traveling in different directions. In this case, the source compensation method takes only (source) amplitude variation in different directions into account, which should effectively remove the undesired effect caused by directive sources used in immersive wave experimentation [8]. The wave phase variation in different directions from a directive physical source is often quite weak or even negligible [7].

We only measure the radiation pattern of a single source and assume the radiation pattern only varies little among the batch of sources such that the measured radiation pattern and further computed directive matched filters can be

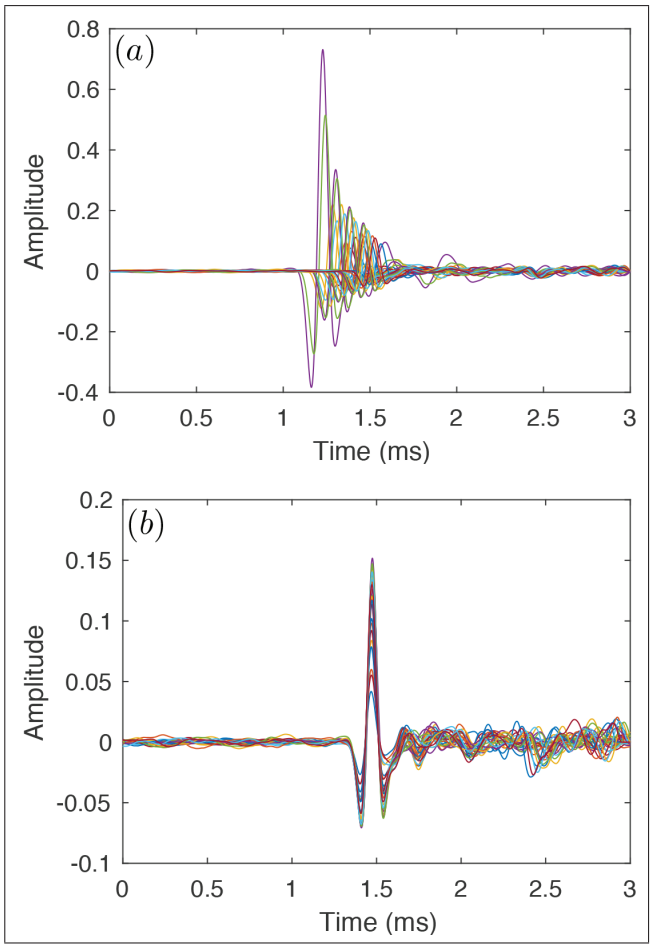

Figure 7. (a) Pressure data recorded with the geometry shown in Figs. 4 and 5. (b) Redatumed data at a uniform radius $r_0 = 0.45$ m with the geometry shown in Fig. 2.

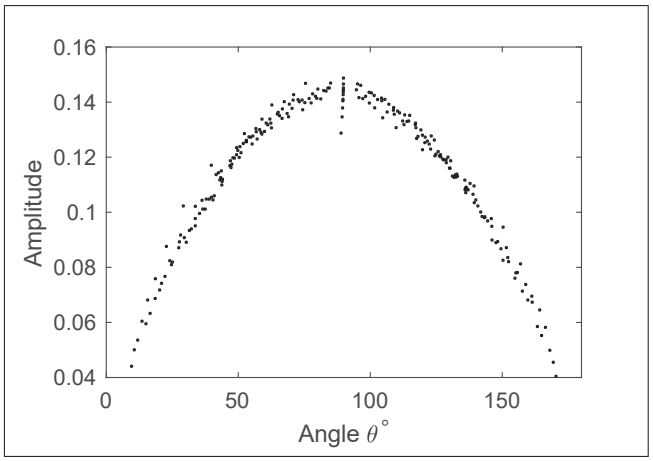

Figure 8. The source radiation pattern of the BMX source.

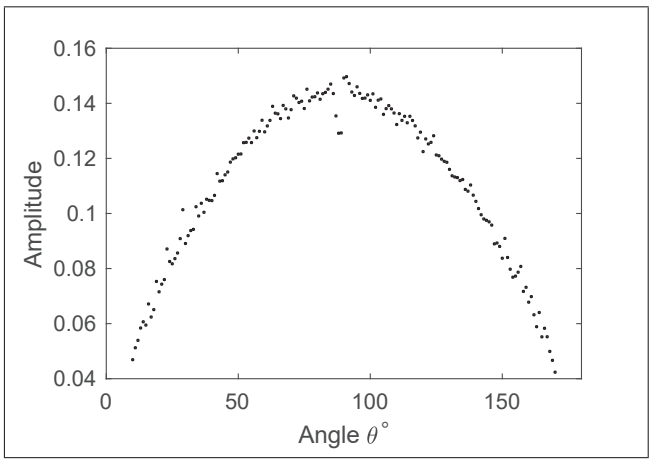

Figure 9. The source radiation pattern of the BMX source including interpolation of the acquired data to yield evenly spaced angles θ.

used to compensate for the directivity of all the sources. In the future laboratory work, we will first test whether this radiation pattern is consistent enough across all the BMX sources. Alternatively, the directivity compensation method still holds if radiation patterns are different for all sources (with some modification, see Ref. [8]). Since the sources need to be mounted on the rigid steel boundary to be measured with the radiation patterns, we need a more effective acquisition geometry or scheme for the measurement, considering that the water tank is limited with its size, and we should avoid boundary reflection present in the data for radiation patterns.

The amplitude radiation pattern, shown with data points in Fig. 8, contains some outliners. The data points that deviate from the general trend of the radiation pattern (for $\theta = 90°$) correspond to the receivers closest to the source. However, no near-source effect theoretically exists in acoustic pressure recordings from a point source [18]. These deviations may be caused by the fact that the physical source has a finite dimension and cannot be considered as a perfect point source. This issue remains to be investigated in the laboratory, but currently, we can remove these data points as outliers.

5. OUTLOOK

We presented the measured radiation pattern of a custom-built BMX-type source in an underwater acoustics laboratory. The source radiation pattern is significantly non-isotropic, which does not fit into the requirement of monopoles in the theory for immersive wave experimentation. In the next step, we will first finish the implementation of the single-sided immersive boundary condition in a 3-D water tank, shown as in Fig. 3(a). Then we assess the effect caused by source directivity, especially when using high emitting frequencies ($>$ 2kHz). We can incorporate our measured source radiation pattern into immersive wave experimentation using the theory proposed in Ref. [8]. We might repeat measurements at some point once we can get rid of the ringing effect for the current BMX sources such that the phase variation in different directions can also be compensated. Finally, we will demonstrate the f-k compensation method in the real laboratory in one-sided/full 3-D experiments.

6. ACKNOWLEDGMENTS

This project has received funding from the European Research Council (ERC) under the European Union's Horizon 2020 research and innovation programme (grant agreement No 694407).

7. REFERENCES

[1] M. Vasmel, J. O. A. Robertsson, D.-J. van Manen, and A. Curtis, "Immersive experimentation in a wave propagation laboratory," *J. Acoust. Soc. Am.*, vol. 134, no. 6, pp. EL492–EL498, 2013.

[2] D.-J. van Manen, J. O. A. Robertsson, and A. Curtis, "Exact wave field simulation for finite-volume scattering problems," *J. Acoust. Soc. Am.*, vol. 122, no. 4, pp. EL115–EL121, 2007.

[3] D. Givoli and D. Cohen, "Nonreflecting boundary conditions based on kirchhoff-type formulae," *J. Comput. Phys.*, vol. 117, no. 1, pp. 102 – 113, 1995.

[4] T. S. Becker, D.-J. van Manen, C. M. Donahue, C. Bärlocher, N. Börsing, F. Broggini, T. Haag, J. O. A. Robertsson, D. R. Schmidt, S. A. Greenhalgh, and T. E. Blum, "Immersive Wave Propagation Experimentation: Physical Implementation and One-Dimensional Acoustic Results," *Phys. Rev. X*, vol. 8, no. 3, p. 031011, 2018.

[5] T. Becker, N. Börsing, D.-J. van Manen, T. Haag, C. Donahue, and A. Curtis, "Immersive wave propagation experiments in a two-dimensional acoustic waveguide," No. 146 (4), p. 3078, 2019. ASA Annual Meeting 2019; Conference Location: San Diego, CA, USA; Conference Date: 2. - 7.12.2019.

[6] T. S. Becker, N. Börsing, T. Haag, C. Bärlocher, C. M. Donahue, A. Curtis, J. O. A. Robertsson, and D.-J. van Manen, "Real-time immersion of physical experiments in virtual wave-physics domains," *Phys. Rev. Applied*, vol. 13, p. 064061, Jun 2020.

[7] N. Börsing, *Acoustic immersive experimentation through real-time control of boundary conditions*. PhD thesis, ETH Zurich, 2019.

[8] X. Li, J. Robertsson, A. Curtis, and D.-J. van Manen, "Compensating for source directivity in immersive wave experimentation," *The Journal of the Acoustical Society of America*, vol. 146, no. 5, pp. 3141–3158, 2019.

[9] F. Broggini, M. Vasmel, J. O. A. Robertsson, and D.-J. van Manen, "Immersive boundary conditions: Theory, implementation, and examples," *Geophysics*, vol. 82, no. 3, pp. T97–T110, 2017.

[10] D. A. B. Miller, "On perfect cloaking," *Opt. Express*, vol. 14, no. 25, pp. 12457–12466, 2006.

[11] E. Willard, "Acoustic Transducer Design for Active Reflection Cancellation in a Finite Volume Wave Propagation Laboratory," Master's thesis, THE UNIVERSITY OF TEXAS AT AUSTIN, 2019.

[12] E. Willard, M. R. Haberman, D.-J. van Manen, J. O. Robertsson, T. S. Becker, and N. Börsing, "Acoustic transducer design for active reflection cancellation in a finite volume wave propagation laboratory," *J. Acoust. Soc. Am.*, vol. 144, no. 3, pp. 1759–1759, 2018.

[13] J. L. Delany, "Bender transducer design and operation," *The Journal of the Acoustical Society of America*, vol. 109, no. 2, pp. 554–562, 2001.

[14] C. Wapenaar and A. Berkhout, *Elastic Wave Field Extrapolation: Redatuming of Single- and Multi-Component Seismic Data*. ISSN, Elsevier Science, 1989.

[15] G. Korn and T. Korn, *Mathematical Handbook for Scientists and Engineers: Definitions, Theorems, and Formulas for Reference and Review*. Dover Civil and Mechanical Engineering Series, Dover Publications, 2000.

[16] MathWorks, "Interpolation for 2-d gridded data in meshgrid format." `https://www.mathworks.com/help/matlab/ref/interp2.html`, 2019.

[17] L. Cheregi, "A comparison between akima and hermite type cubic spline with minimal quadratic oscillation in average," 2018.

[18] G. Parkes and L. Hatton, *The Marine Seismic Source*. Modern Approaches in Geophysics, Springer Netherlands, 1986.